Theoretical and Applied Fracture Mechanics 133 (2024) 104607

Contents lists available at ScienceDirect

Theoretical and Applied Fracture Mechanics

journal homepage: www.elsevier.com/locate/tafmec

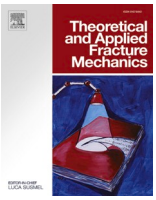

The Smith-Watson-Topper parameter and fracture surface topography relationship for additively manufactured 18Ni300 steel subjected to uniaxial variable-amplitude loading

Wojciech Macek [a,b,*], Zbigniew Marciniak [c], Grzegorz Lesiuk [d], Przemysław Podulka [e], Cho-Pei Jiang [f]

[a] Faculty of Mechanical Engineering and Ship Technology, Gdańsk University of Technology, Narutowicza 11/12, 80-233 Gdańsk, Poland
[b] Advanced Materials Center, Gdańsk University of Technology, Narutowicza 11/12, 80-233 Gdańsk, Poland
[c] Opole University of Technology, Department of Mechanics and Machine Design, Mikolajczyka 5, 45271 Opole, Poland
[d] Faculty of Mechanical Engineering, Wroclaw University of Science and Technology, Smoluchowskiego 25, 50-370 Wrocław, Poland
[e] Faculty of Mechanical Engineering and Aeronautics, Rzeszow University of Technology, Powstancow Warszawy 12, 35-959 Rzeszów, Poland
[f] Department of Mechanical Engineering, National Taipei University of Technology, Taipei 10608, Taiwan

ARTICLE INFO

Keywords:
18Ni300 steel
Laser beam powder bed fusion
Fatigue
Variable-amplitude loading
Surface topography
Entire fracture surface method
Smith-Watson-Topper parameter

ABSTRACT

In this paper, the association between Smith-Watson-Topper (SWT) parameter and fracture surface topography is studied in additively manufactured maraging steel exposed to variable-amplitude fatigue loading. The post-failure fracture surfaces were examined using a non-contact 3D surface topography measuring system and the entire fracture surface method. The focal point is on the correspondence between fatigue characteristics, articulate by the SWT parameter, and the fracture surface topography features, represented by areal, volume, and fractal dimension parameters. A fatigue life prediction model based on SWT and fracture surface topography factors is proposed. The presented model expresses good compliance with fatigue test results. This model can be useful for post-mortem analysis of engineering elements under variable-amplitude loading fatigue, especially for materials produced by additive manufacturing (AM).

1. Introduction

Additive Manufacturing, initiated in the 1980 s, is a pioneering technique for the production of 3D items across the layer-by-layer deposition of material [1]. Metal-based additive manufacturing appears for a group of processes that usually include powder bed fusion (PBF), directed energy deposition (DED), sheet lamination, and binder jetting [2]. Inside this group, laser beam powder bed fusion (LB-PBF) is nowadays one of the most popular processes [3]. The 18Ni300 maraging steel, as a type of low-carbon iron-nickel alloy with high strength and toughness, has been indicated to be appropriate for LB-PBF [4].

The mechanical properties, including fatigue life, are influenced by the manufacturing parameters and printing orientation effects [5,6]. Fatigue response is critical in most engineering applications subjected to cyclic loading [7,8]. Research of this type for additive manufactured 18Ni300 maraging steel was previously conducted by Karolczuk et al. [9]. The Authors investigate the heterogeneous effect of ageing temperature on the fatigue life of tubular specimens. The mechanical properties of tubular specimens were close to or higher than those of a full cross-section geometry. Solberg et al. [10] investigate the influence of specimen orientation on fatigue behaviour and propose a new test methodology for evaluating up- and down-skin fatigue. They found that build orientation correlates to the specimen's surface roughness.

Surface topography is commonly used to discuss and explain damage mechanisms occurring during deformation [11]. AM material roughness affects fatigue strength very strongly, which was shown in Sanaei and Fatemi's paper [12]. They proved that fatigue limit increases with a decrease in surface roughness regardless of the microstructure. Bai et al. [13] analyse the influence mechanism of process parameters on the surface quality and internal hole defect generation of 18Ni300 steel. The authors showed, among other things, that increasing the volumetric energy density improves the surface's quality and, consequently, the mechanical properties. Romano et al. [14] discuss how surface defects influence fatigue results. In the same paper, the researchers also

* Corresponding author.
E-mail address: wojciech.macek@pg.edu.pl (W. Macek).

https://doi.org/10.1016/j.tafmec.2024.104607
Received 1 April 2024; Received in revised form 3 August 2024; Accepted 5 August 2024
Available online 6 August 2024
0167-8442/© 2024 The Author(s). Published by Elsevier Ltd. This is an open access article under the CC BY license (http://creativecommons.org/licenses/by/4.0/).

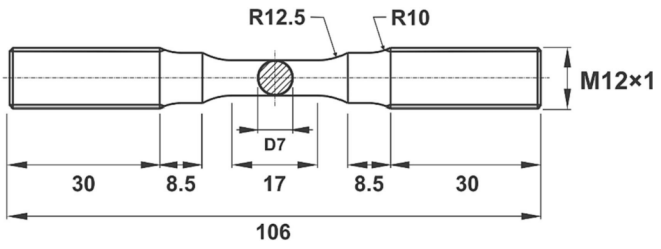

Fig. 1. Specimen geometry used in the fatigue tests [25].

examined fracture surfaces. They proved a significant obvious improvement of HCF properties for specimens after machining, but they also found the improvement in fatigue life to be related to increasing the machining allowance.

With the development and availability of advanced techniques and methods for measuring surface topography, it has become common not only to quantify the lateral surfaces of specimens, but also their fractures after failure [15,16]. Newly discovered methods of analyzing surface topography, such as raw data thresholding technique, digital filtering (S-filter), power spectral density, and autocorrelation function analyses by Podulka et al. [17] or fractal dimension by Macek et al. [18] also contribute to the development of 3D fractography. Fast Fourier Transform with Murakami formula has been applied for study effect of the surface roughness on the fatigue life by Macoretta et al. [19]. Statistical classification for estimating the fatigue crack growth rate on the basis of 3D features of fracture surfaces has been proposed by Lauschmann et. al [20,21]. They examined global area parameters, line profile parameters and local (point) parameters and successfully performed a fractographic reconstitution of the history of fatigue crack growth.

A deep understanding of failure mechanisms and fracture surface topography relationships is actually a great challenge in the field of materials science. Macek et al., for example in papers [29,32,33] successfully use the Entire fracture surface method to analyze the fatigue fracture surface topography. Using the measurement results on various 3D measuring machines, the fracture surfaces of various materials loaded in different ways were analyzed. This method is universal and has shown promising results for further development.

The second inspiration for this investigation is based on earlier research, involving modeling using the SWT fatigue damage parameter [22] or wider, strain energy density parameters [23,24]. Smith-Watson-Topper parameter was partially used to estimate fatigue life for the same set of specimens by Marciniak et al. [25]. The Palmgren-Miner damage rule along with the SWT parameter provided consistent fatigue life predictions. Macek et al. [26] proposed the total strain energy density combined with the entire fracture surface parameters, which showed a

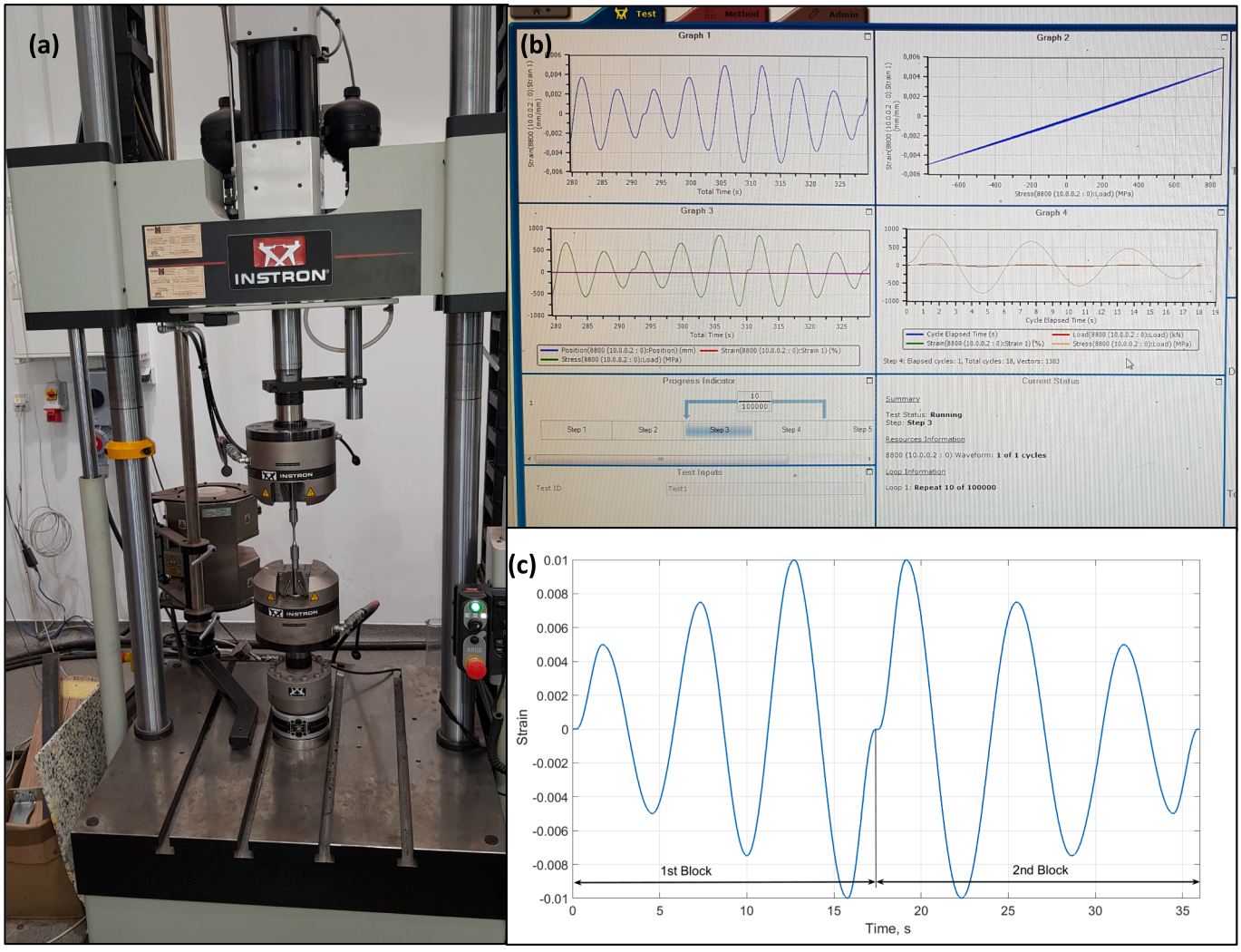

Fig. 2. (a) Universal servo-hydraulic testing system, model Instron 8802, used in fatigue tests; (b) fatigue test control panel; (c) details of the loading sequence considered in the fatigue tests for the test with maximum strain amplitude of 1.00 %. Ascending cycles with strain amplitudes of 0.50 %, 0.75 %, and 1.00 % (1st block) and descending cycles with strain amplitudes of 1.00 %, 0.75 %, and 0.50 % (2nd block).

MOST WIEDZY Downloaded from mostwiedzy.pl

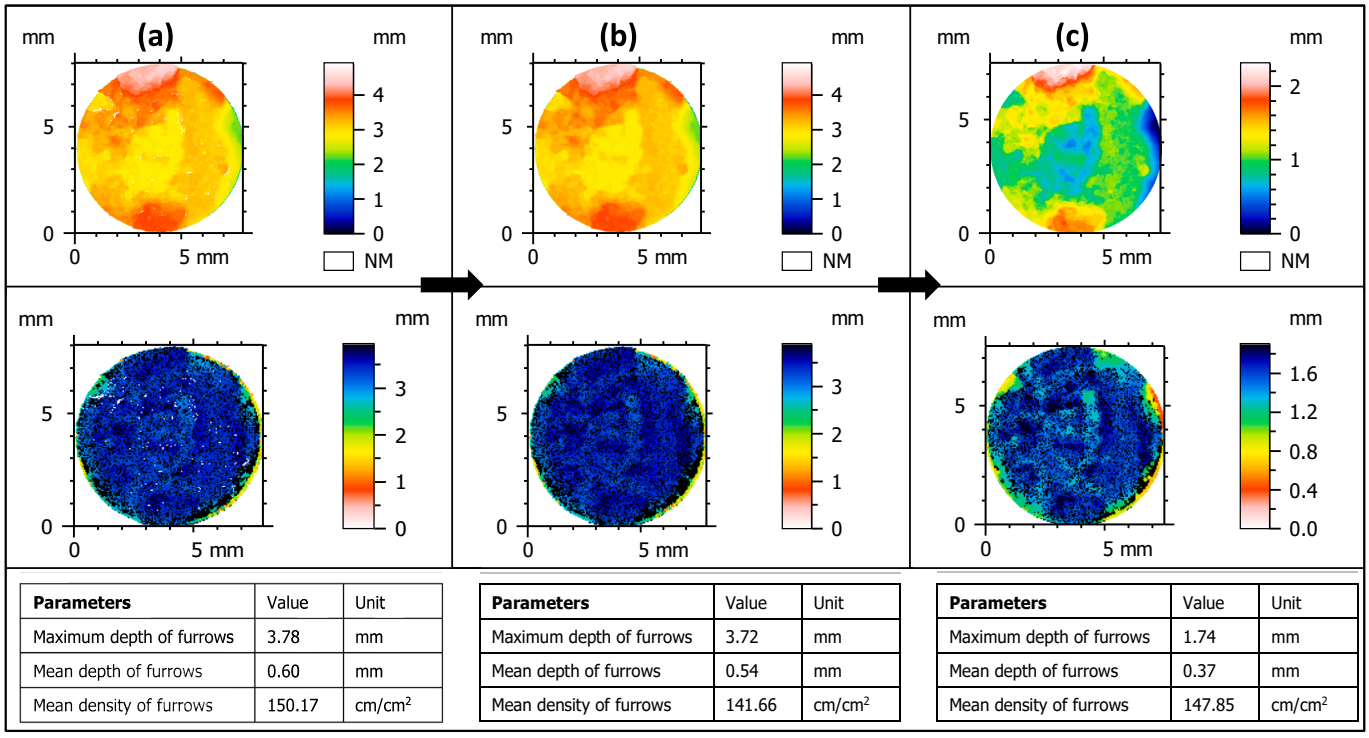

Parameters	Value	Unit
Maximum depth of furrows	3.78	mm
Mean depth of furrows	0.60	mm
Mean density of furrows	150.17	cm/cm^2

Parameters	Value	Unit
Maximum depth of furrows	3.72	mm
Mean depth of furrows	0.54	mm
Mean density of furrows	141.66	cm/cm^2

Parameters	Value	Unit
Maximum depth of furrows	1.74	mm
Mean depth of furrows	0.37	mm
Mean density of furrows	147.85	cm/cm^2

Fig. 3. Entire fracture surface methodology processing: (a) original fracture surface; (b) the NMP filling surface, and (c) extracted fracture surface.

satisfactory relationship with the fatigue life, following a power-law.

As part of this work, the following were examined: (1) variable amplitude fatigue tests, the results of which were initially presented in [25]; (2) estimation of fatigue life using the SWT parameter, partially presented by the authors, also in [25]; (3) results of measurements and analysis using the *entire fracture surface* method, partially described in [25]; and (4) a proposal for a new approach to estimating fatigue life, combining the SWT parameter (2) and fatigue fracture surface topography indicators (3).

2. Material and methods

2.1. Material preparation

Round cross-section specimens were made from 18Ni300 maraging steel manufactured by laser beam powder bed fusion in vertical direction with a depth layer of 40 μm (see Fig. 1). The speed scan was 200 mm/s with a maximum power of 100 W. Chemical composition of the tested material is: 0.03 % C, 18.2 % Ni, 0.7 Ti, 9 % Co, 4.8 % Mo, 0.1 % Al, 0.3 % Cr, 0.01 % P, 0.1 % Si, 0.01 % S and Fe balance. The microstructure contains elongated grains with an average length of 150 μm and a width of 35 μm. The structure is characterized by small porosity of 0.71 %.

2.2. Material testing

All signals for strain and stress were collected using the Instron System in a 100 kN closed-loop servo-hydraulic testing machine, model Instron 8802 (see Fig. 2(a)). The main set parameters are presented on the control panel in Fig. 2(b). Variable amplitude loading tests were performed with strain-controlled conditions ($R_\varepsilon = -1$) at room temperature. Loading sequences consist of two blocks with 3 different amplitudes of strain each (see Fig. 2(c)). The amplitudes in the first block increased and they decreased in the second one. The amplitudes have 50 %, 75 % and 100 % of the maximum value of amplitude. Four levels of loadings were selected according to maximal value of strain amplitude $\varepsilon_{a,max}$: 0.35 %, 0.5 %, 0.75 % and 1 %. The amplitudes were selected to conduct tests in low cycle fatigue (LCF) and high cycle fatigue (HCF) as well [25].

2.3. Fracture surface measurement

The fracture surface analysis refers to a two-phase process: (1) we have to acquire the topographical data of the irregular fracture surface, and (2) using the entire fracture surface method, this irregular surface factor is obtained using various surface topography parameters.

The examination of fracture surfaces was carried out for both sides of the broken specimens, which gave a total of 24 analyzed entire fracture surfaces. However, the results of the surface topography parameters for both sides of the 12 specimens were similar, which was also shown for other studies as [27], the average results from both sides were used for further analyses. The fracture surfaces were measured using the vision measuring system MITUTOYO QV Apex 302 [25]. The fractures were observed under 5 × magnification with a 1.24 × 0.93 mm^2 field of view and were stitched together to map the entire fracture area, with a total resolution scale of 0.1 μm. Mitutoyo (*.Q3D) source files were transferred into the surface texture analysis software MountainsMap and resampled into height maps at a resolution automatically set by the software.

The whole surface was reduced to eliminate the regions associated with the geometric discontinuities or missing points, as well as to obtain uniform dimensions for all specimens. An example of the entire process is shown in Fig. 3. The surface was limited to a circle with a diameter of 7.5 mm, by the maximum strain amplitude of 0.35 %. The original surface is shown in Fig. 3(a), the non-measured points (NMP) [28] filling is presented in Fig. 3(b), and the final extracted surface is displayed in Fig. 3(c). Below the visualization of the appropriate surfaces, the Furrows plot [21] displays all furrows and results for maximum furrow depth, mean furrow depth, and furrows' mean density are presented.

Additionally, the surface analysis was supported by SEM fractographs taken by model Zeiss Merlin 13 FE-SEM, with high and low magnifications.

MOST WIEDZY Downloaded from mostwiedzy.pl

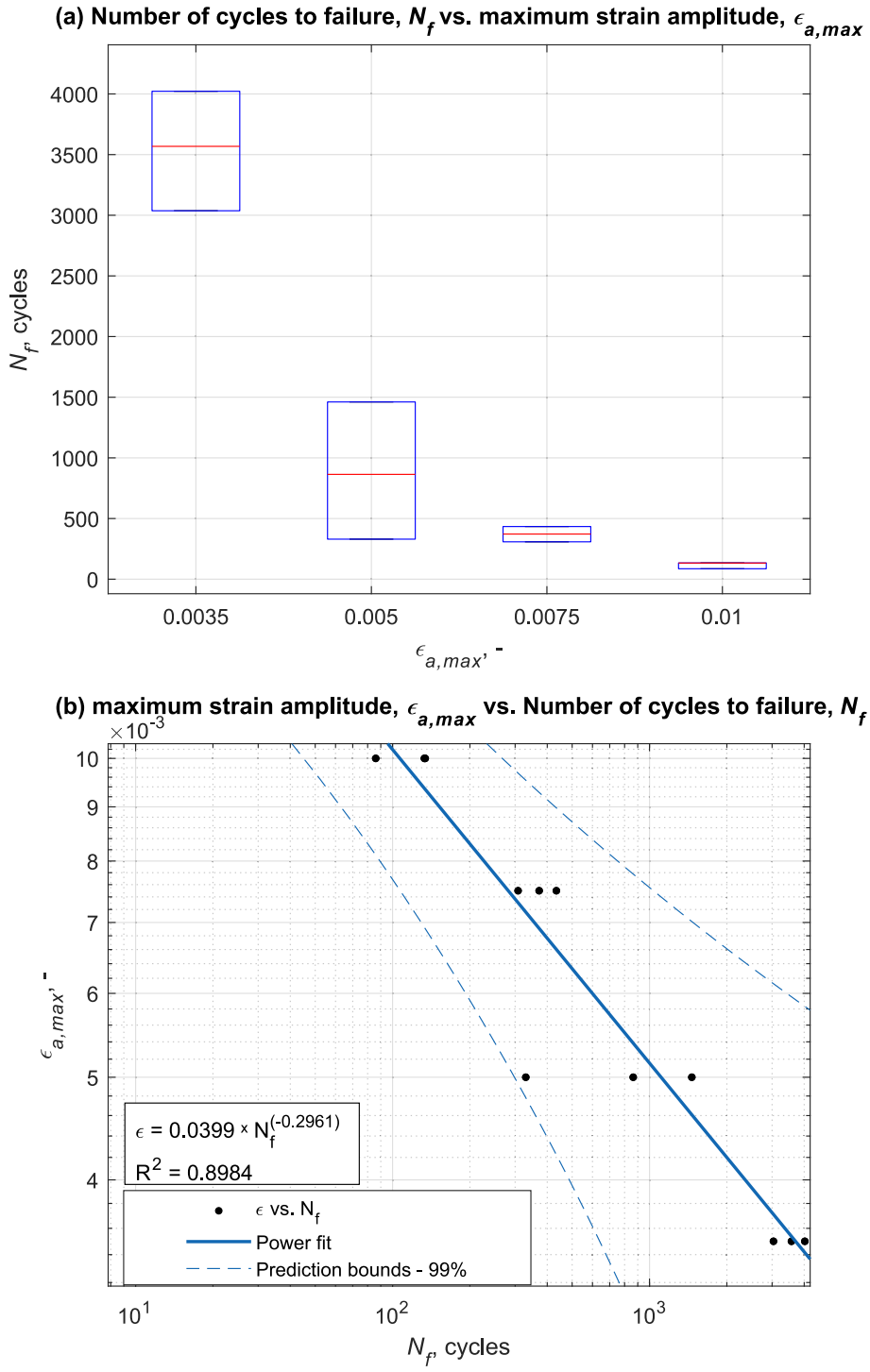

Fig. 4. Fatigue life against the maximum strain amplitude of the loading scenario in form: (a) boxplot, and (b) curve fitting tool.

MOST WIEDZY Downloaded from mostwiedzy.pl

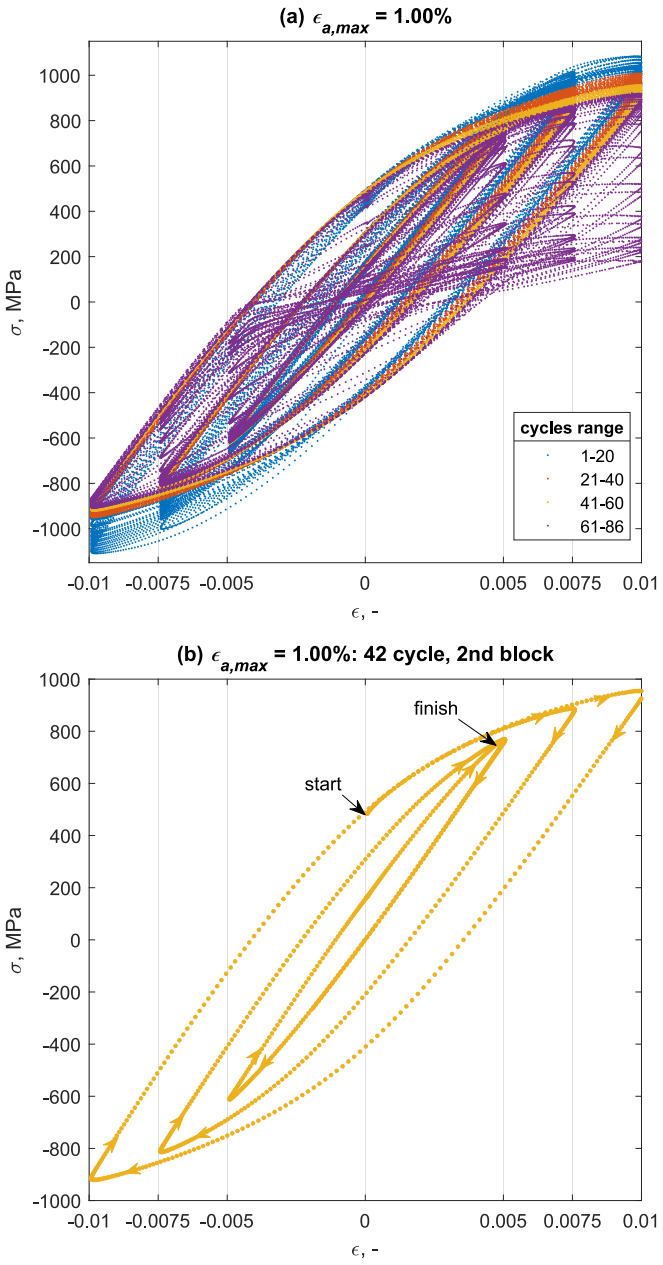

Fig. 5. Example of the hysteresis loops collected in the tests at a maximum strain amplitude of 1 %: (a) for all stages of fatigue life; (b) for one cycle (42) – 2nd block of fatigue life.

Table 1
Summary of fatigue tests performed under variable-amplitude loading [25].

$\varepsilon_{a,1}$ (%)	$\sigma_{max,1}$ (MPa)	$\sigma_{min,1}$ (MPa)	$\varepsilon_{a,2}$ (%)	$\sigma_{max,2}$ (MPa)	$\sigma_{min,2}$ (MPa)	$\varepsilon_{a,3}$ (%)	$\sigma_{max,3}$ (MPa)	$\sigma_{min,3}$ (MPa)	N_f (cycles)
1.00	760.8	−666.7	0.75	876.5	−864.2	0.50	933.6	−974.0	134
1.00	743.5	−656.6	0.750	852.6	−849.8	0.50	916.3	−962.5	133
1.00	769.9	−611.3	0.750	888.0	−813.8	0.50	954.7	−920.9	86
0.75	616.7	−514.1	0.563	784.9	−748.3	0.38	897.6	−913.6	434
0.75	375.8	−440.7	0.563	606.9	−521.6	0.38	888.4	−931.3	372
0.75	375.8	−440.7	0.563	621.0	−529.2	0.38	908.9	−937.2	308
0.50	476.9	−344.5	0.375	668.0	−554.3	0.25	846.8	−755.2	864
0.50	625.9	−166.3	0.375	810.0	−363.4	0.25	983.0	−555.4	330
0.50	375.8	−440.7	0.375	565.6	−648.1	0.25	742.1	−848.2	1461
0.35	331.0	−226.3	0.263	464.42	−400.2	0.18	599.2	−518.3	4022
0.35	308.5	−258.9	0.263	445.79	−403.5	0.18	583.1	−548.4	3037
0.35	237.1	−338.0	0.263	377.05	−483.6	0.18	516.2	−631.6	3568

MOST WIEDZY Downloaded from mostwiedzy.pl

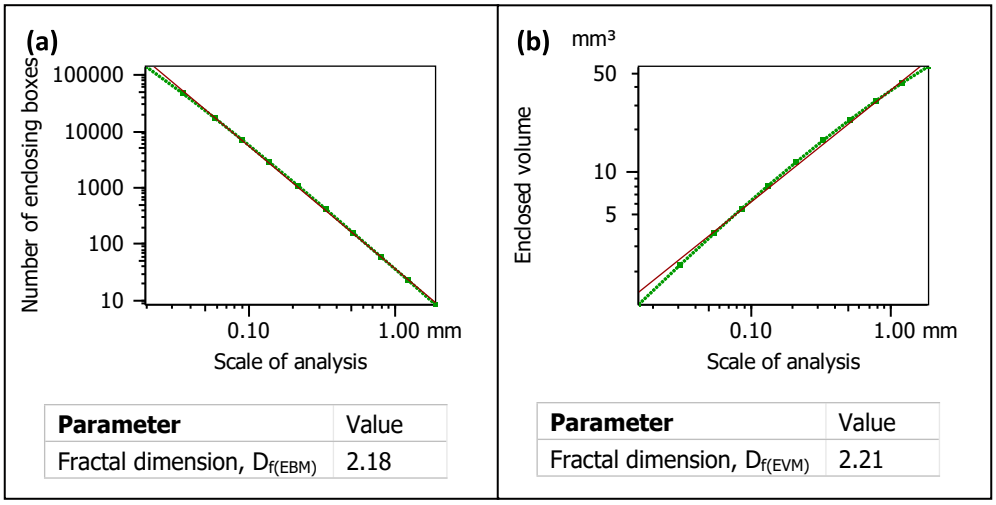

Fig. 6. Example of graphical representations of fractal dimension in the tests at a maximum strain amplitude of 0.75 % for: (a) enclosing boxes method, $D_{f(EBM)}$; (b) morphological envelope method $D_{f(EVM)}$.

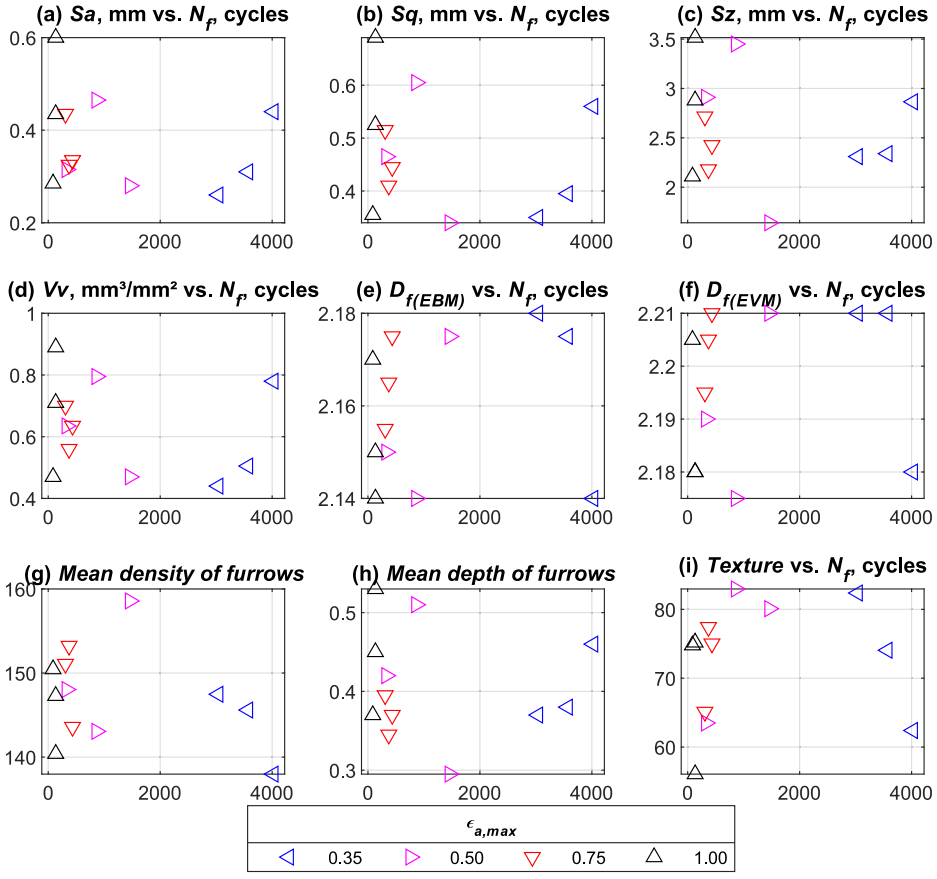

Fig. 7. Standard and non-standard surface topography parameters in relation to fatigue life N_f: (a), (b).

2.4. Smith-Watson-Topper (SWT) parameter

In literature there exist a lot of fatigue criteria: (i) stress-based criteria, (ii) strain-based criteria and (iii) energy-based criteria. Depending on the cyclic behaviour of materials and time history, the researchers use them to correlate fatigue parameters versus fatigue life. One of the best-known and often used ones is the Smith-Watson-Topper parameter ($SWT = \sigma_{max}\ \varepsilon_a$). This model includes stress and strain histories and is suitable for non-zero mean stress.

3. Results

3.1. Mechanical testing

The variable-amplitude fatigue test results have been presented in Fig. 4 and have been analysed according to the boxplot (see Fig. 4(a)), as well as the curve fitting tool (see Fig. 4(b)). For boxplot on each box, the central mark indicates the median. For the curve fitting tool (Fig. 4(b)), power fit was the best fit, with a coefficient of determination, R^2 =

MOST WIEDZY Downloaded from mostwiedzy.pl

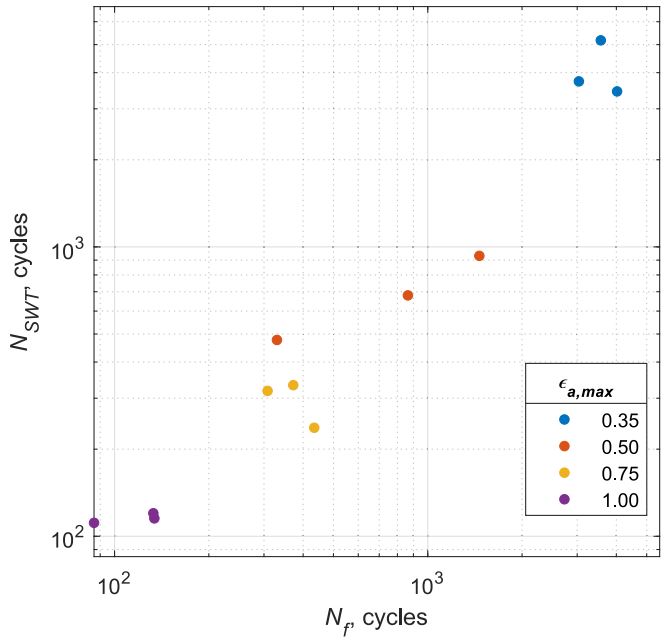

Fig. 8. Predicted fatigue life (N_{SWT}) against the experimental fatigue life (N_f).

0.8984.

The stress response acquired in the fatigue tests with VA loading accomplished under fully-reversed strain cycles is shown in Fig. 5. Fig. 5a shows how stress changed during the test, and the mean stress also changed.

Table 1 provides a summary of the main stress and strain variables of each cycle of the first block for the half-life.

3.2. Fracture surface analysis

A total of 24 surfaces resulting from 12 analyzed specimens subjected to fatigue tests were analyzed. Individual parameters were averaged for each specimen from both sides of the broken specimen.

The main fractographic features should be well reflected by the surface topography parameters. There are standard and non-standard parameters. The first type of parameters is defined in the ISO 25178 Standard. It includes two groups, height and volume parameters denoted as *Sx* and *Vx*, respectively. Finally, root mean square height, *Sq* and arithmetic mean height, *Sa* was selected as the best-fitting parameters for these groups. Root mean square height, *Sq* and arithmetic mean height, *Sa* are defined by the Eqs. (1) and (2), respectively.

$$Sq = \sqrt{\frac{1}{A}\iint_A z^2(x,y)dxdy} \tag{1}$$

$$Sa = \frac{1}{A}\int_A |z(x,y)|dxdy \tag{2}$$

where A is the definition area; z is the surface height in position x , y; x and y are the lengths in the perpendicular directions.

Among the non-standard parameters, one can indicate the fractal dimension, D_f, used to examine the surface topography with no additional filters. Fractal dimension $D_{f(EBM)}$ for enclosing boxes method breaks up the area into subareas with a width δ and computes the size ($V\delta$) of all volumes overlaying the whole area. Whereas fractal dimension $D_{f(EVM)}$ morphological envelope method captures the upper and lower envelopes, which are considered by morphological opening and closing, defining a composition component which assumes the form of a horizontal line segment with length δ [29]. A slope of the fitted line corresponds to D_f calculated as the absolute, as shown in Fig. 6.

The next parameters taken into account are resulting furrow renderings, as mentioned in subsection 2.3 (see Fig. 3), which were obtained through the Fourier transform applied by MountainsMap on topographic height functions. They simulate furrows around the peaks and valleys along the surface for better qualitative visualization of the fracture surface morphology. The surface topography analysis complements a texture isotropy study, which pointed to calculating the isotropy parameters with respect to a threshold, assumed equal to 0.20. These values allowed to quantify the central zones corresponding to the portion of the peaks that remained after thresholding [26].

The results of the mentioned standard and non-standard surface topography parameters concerning fatigue life are summarized in Fig. 7.

3.3. Smith-Watson-Topper parameter versus fatigue life

Relating to the non-zero mean stress effects, the Smith-Watson-Topper (SWT) parameter [30] was used, considering the corrections of both the elastic and plastic terms:

$$SWT = \varepsilon_a \sigma_{max} = \frac{\left(\sigma_f'\right)^2}{E}(2N_f)^{2b} + \sigma_f'\varepsilon_f'(2N_f)^{b+c} \tag{3}$$

where ε_a is the strain amplitude, σ_{max} is the maximum stress, σ_f' is the fatigue strength coefficient, b is the fatigue strength exponent, ε_f' is the fatigue ductility coefficient, c is the fatigue strength exponent, N_f is the fatigue life, and E is Young's modulus.

In relation to the cumulative fatigue damage, it was accounted for by using the linear Palmgren-Miner damage rule [31]:

$$\sum_{i=1}^{k}\frac{n_i}{N_i} = 1 \tag{4}$$

where n_i the number of cycles applied at the i^{th} loading level, and N_i is the fatigue life at the i^{th} loading level.

The fatigue life predicted by applying the SWT parameter in conjunction with the Palmgren-Miner damage rule, as well as the experimental fatigue life obtained in the variable-amplitude fatigue tests, are presented in Fig. 8. Predicted fatigue life (N_{SWT}) against the experimental fatigue life (N_f).

3.4. Fractographic SEM observations

The analysis of the fractographic view of the fractured 18Ni300 after variable-amplitude loading was carried out. Both figures were related to the specific maximum strain amplitude: Fig. 9(a) of $\varepsilon_{a,\max} = 1$ %, and Fig. 9(b) of $\varepsilon_{a,\max} = 0.50$ %.

The crack nucleation region of the specimen can be observed at the edge of the specimen's cross-section. Both the observed surfaces demonstrated three characteristic areas: crack initiation area, stable crack propagation area, and the final ductile fracture area. After the initiation stage, cracks propagated through the cross-section. An increase of the strain amplitude led to a slight change in the fracture nature. Also, some defects in the form of many small voids and cracks can be identified, which could be the reason for the accelerated damage. Since unmelted powders or unfused particles were discovered in the structure, this might have been caused by some manufacturing process instability.

4. Discussion

Previously, several modifications to the SWT parameter have been proposed [32]. The authors of this paper also attempted to find a correlation between the parameter related to widely understood strain energy or stress level and the fatigue fracture surface parameters (post-failure). In paper [33] the authors studied the effect of creep pre-strain

MOST WIEDZY Downloaded from mostwiedzy.pl

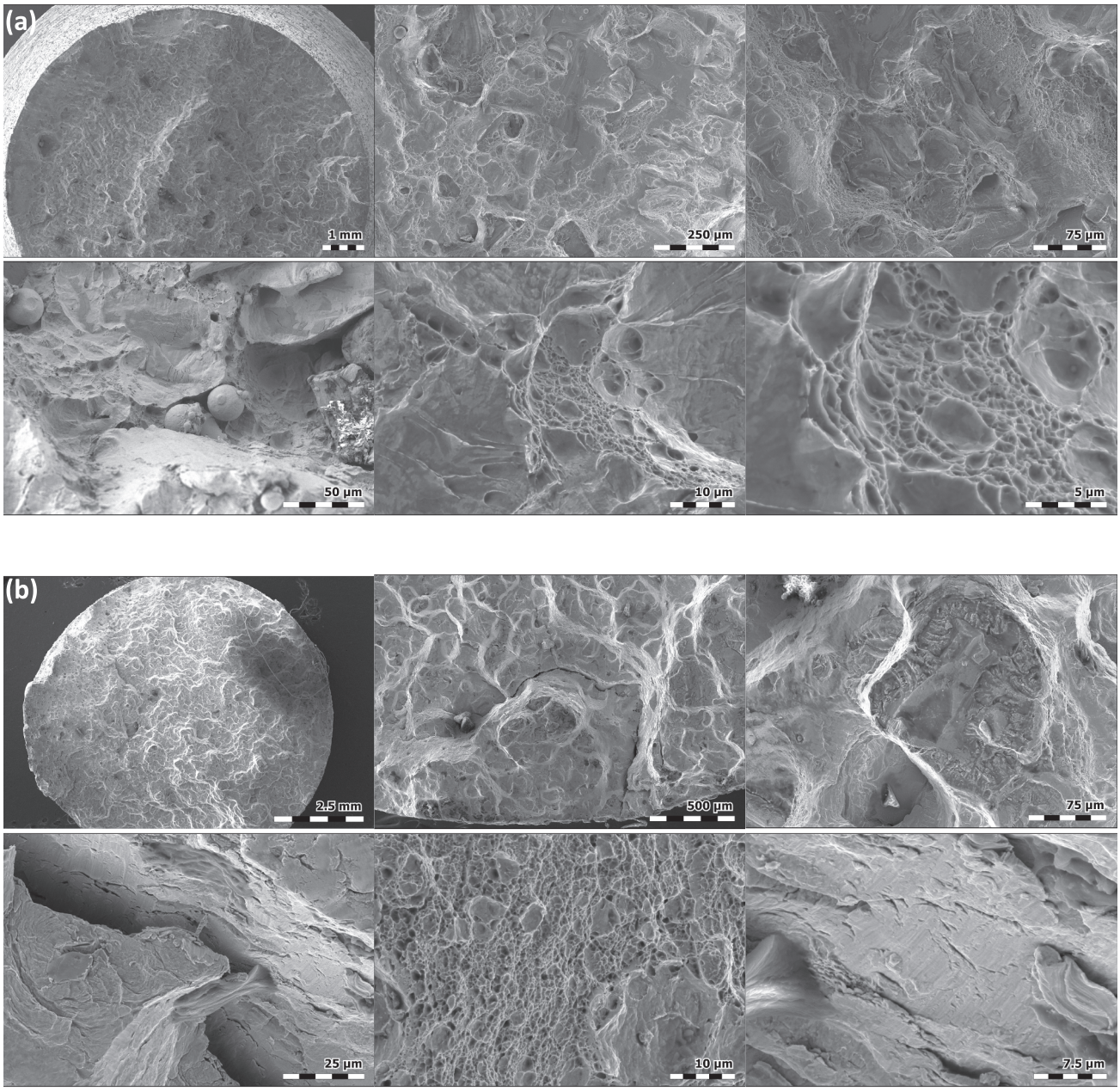

Fig. 9. SEM images of the entire fracture surface generated in the variable-amplitude fatigue tests for a maximum strain amplitude of: (a) 1.00 %; and (b) 0.50%.

on LCF failure via fractographic analysis for EN-AW 2024 AA. They proposed a new damage parameter P [33] combining fracture surface topography and load features (see Eq. (5)).

$$P_{[33]} = \frac{VvD_f}{Sq} \times \varepsilon_a \sigma_a + \varepsilon_{creep} \times \sigma_{creep} \tag{5}$$

which combines the three topography characteristics (i.e. height parameter Sq, the functional parameter Vv, and the fractal dimension D_f) with both the strain amplitude ε_a and the stress amplitude σ_a, as well as the creep strain ε_{creep} and the creep stress σ_{creep}.

The authors in [27] proposed another variation of the P [27] parameter (see. Eq. (6)) applicable for notched aluminum alloys under bending load.

$$P_{[27]} = \frac{Sq}{Sa} \times (D_f + R) \times \sigma_{max}(\text{MPa}) \tag{6}$$

where Sq and Sa are surface topography parameters, D_f is the fractal dimension, R is the stress ratio, and σ_{max} is the maximum bending stress. P [27] parameter aims to reflect three elements: fracture surface topography ($\frac{Sq}{Sa}$); stress ratio modulated by the fractal dimension ($D_f + R$); and the maximum bending stress σ_{max}, respectively.

The case of fatigue crack initiation life, which was successfully predicted from fracture surface parameters and maximum local von Mises stress was dealt with in [34]. In this approach, a new parameter P [34], defined in Eq. (7), was introduced:

$$P_{[34]} = \frac{\sigma_{VM} \times Df}{Sq/Vv} \tag{7}$$

where σ_{VM} is the maximum local equivalent von Mises stress, D_f is the fractal dimension, Sq is the root mean square height, and Vv is the void volume.

MOST WIEDZY Downloaded from mostwiedzy.pl

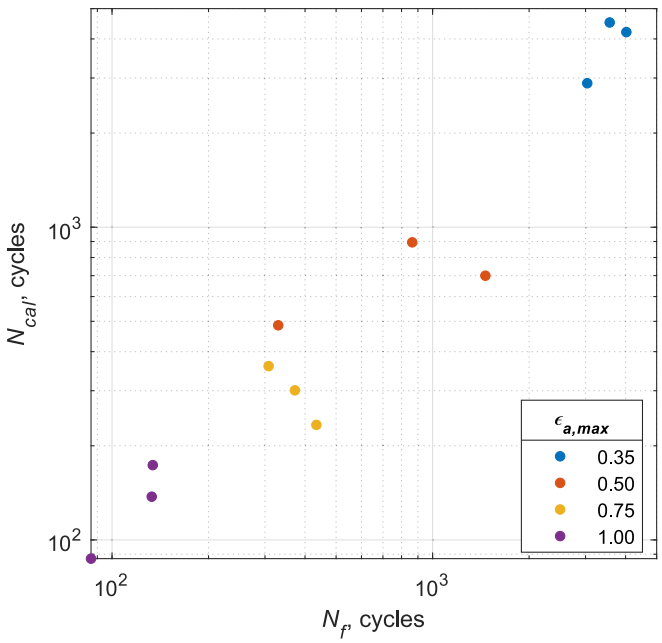

Fig. 10. New prediction model, N_{cal} versus experimental fatigue life N_f.

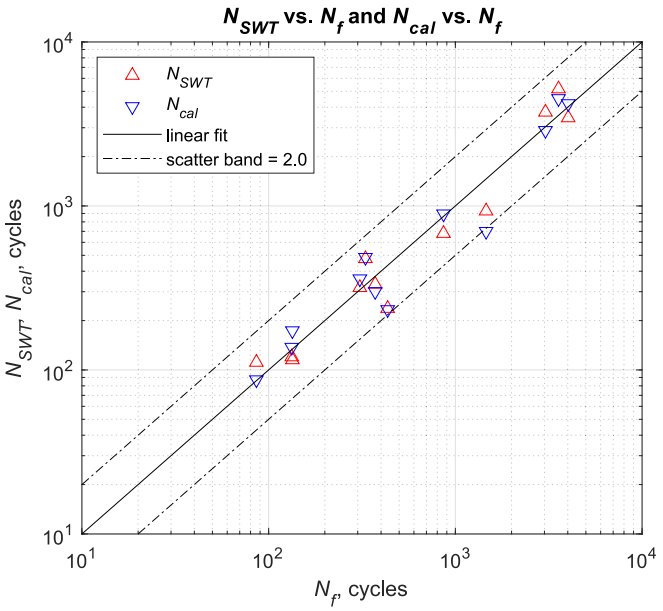

Fig. 11. Experimental fatigue life versus predicted fatigue life for the variable-amplitude fatigue tests, taking into account scatter bands.

Table 2
Fatigue life predictions for the variable-amplitude fatigue tests.

N_f (cycles)	N_{SWT} (cycles)	N_{cal} (cycles)
134	115	173
133	120	137
86	111	87
434	237	233
372	333	301
308	318	360
864	680	895
330	477	486
1461	931	700
4022	3446	4206
3037	3732	2886
3568	5172	4515

Austenitic stainless steel notched specimen fractures were studied, as in previous cases, via the entire fracture area method [35]. The observed N_f and the predicted N_{cal} lifes computed with proposed parameter (see Eq. (8) for the linear model show satisfactory compliance.

$$P_{[35]} = \frac{Sq}{Vv}\sigma_a \tag{8}$$

A fatigue life prediction model based on total strain energy density and fracture surface topography parameters is proposed [26]. The presented model (see eq. (9) shows good accordance with fatigue test results and outperforms other existing models based on the strain energy density.

$$W^* = W \times \frac{Vv \times Df}{Sq} \tag{9}$$

where W is the strain energy density, and W^* is the modified strain energy density.

The proposed damage parameters P (Eqs. (5)–(9)) can successfully estimate the fatigue lifetime. Therefore, in this case, it was also decided to propose a new prediction life method N_{cal}, depending on the SWT parameter and the surface topography of fatigue fractures. In the current approach, a new predicted fatigue life N_{cal} (see Eq. (10)), defined from the $\frac{Sa}{Sq}$ and $D_{f(EVM)}$ multiplied by the N_{SWT}, was introduced. The new post-failure equivalent topographic fracture factor reflects the physical failure conditions of material under fatigue. The new parameter aims to identify the main governing quantities to reflect the physical meaning of the damaging process. The first part represents the fracture surface energy through the combination of three fracture surface topography parameters ($\frac{Sa}{Sq} \times D_{f(EVM)}$). The unit, for this part of the equation, is as follows: [mm/mm × (−)]. The N_{SWT} quantity reflects the fatigue loading history. Therefore, the new prediction model N_{cal}, maintains the same unit as number of cycles to failure, N_f, or predicted fatigue life with classical SWT parameter N_{SWT}, i.e. [cycles] or [-].

Fig. 10 shows the correlation between the new prediction method N_{cal} and the fatigue life for the tested cases.

$$N_{cal} = \frac{Sa}{Sq} \times D_{f(EVM)} \times N_{SWT} \tag{10}$$

Through the analysis of the coefficient of determination R^2, it is possible to conclude that the proposed N_{cal} (for N_{cal} linear fit: $R^2 = 0.9543$) parameter fits the data better than the classical SWT parameter (for N_{SWT} linear fit: $R^2 = 0.9056$).

The fatigue life correlations by applying both the SWT and the modified SWT parameters in conjunction with the experimental fatigue life obtained in the variable-amplitude fatigue tests are presented in Table 2 and Fig. 11. N_{SWT} and N_{cal} were computed through the SWT and modified SWT parameters with Eqs. (2) and (3)) and Eq. (10), respectively.

As can be seen, the calculations with both methods based on SWT parameter correlate well with the experimental results, since all of the tested cases results fall in a 2.0 scatter bands.

In order to better evaluate the predictive capabilities of the tested approaches, a statistical study was formed, based on the prediction bound. Fig. 12 shows that the predictions through the modified SWT parameter model N_{cal} were more accurate than those determined by applying the SWT parameter N_{SWT}. Both predictions are within prediction bounds 99 % (see Fig. 12(a)), but the highest value of N_{SWT} (N_{SWT}=5172 (cycles)) is at the border. However, in terms of durability up to 1000 cycles, the prediction bounds is 50 % (see Fig. 12(b)).

5. Conclusions

The paper presents the comparison of the fatigue life for LB-PBF

MOST WIEDZY Downloaded from mostwiedzy.pl

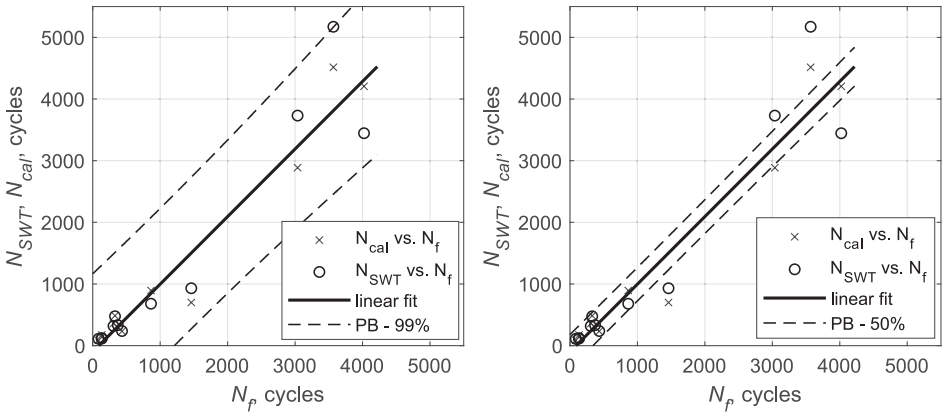

Fig. 12. Experimental fatigue life versus predicted fatigue life for the variable-amplitude fatigue tests, taking into account prediction bounds: (a) 99 %; and (b) 50 %.

18Ni300 maraging steel versus topography parameters. Both methods: based on Smith-Watson-Topper parameter and SWT, taking into account fracture surface topography, were used for comparison. From the present study, the following conclusions can be drawn:

- The new factor included to fatigue life prediction based on SWT parameter defines the fracture surface quality (roughness). Analyses have shown that the parameter's value increases with a decrease in load, directly related to the increase in the specimens' fatigue lives.
- The SWT parameter at the mid-life cycle combined with the entire fracture surface parameters showed a satisfactory relationship with the fatigue life, following a linear fit;
- Predictions made using the SWT-based approaches fell within scatter bands of ± 2.0, the same as those obtained from the modified SWT-based approach. However, the approach taking into account the fatigue fracture surface topography achieved a better coefficient of determination R^2 (linear fit: $R^2 = 0.9543$ vs. $R^2 = 0.9056$);

This methodology holds promise for the application in variable-amplitude life assessment for other additive manufactured metallic materials and can contribute to enhance the understanding of the fatigue failure kinetics.

Linking the topography parameters of the fatigue fracture surface with the SWT parameter and fatigue life may allow the development of a reverse method for estimating load parameters and analysing factors causing damage.

CRediT authorship contribution statement

Wojciech Macek: Writing – original draft, Visualization, Validation, Supervision, Methodology, Investigation, Formal analysis, Data curation, Conceptualization. **Zbigniew Marciniak:** Writing – review & editing, Validation, Resources, Investigation, Data curation. **Grzegorz Lesiuk:** Writing – review & editing, Supervision, Data curation. **Przemysław Podulka:** Writing – review & editing, Software, Data curation. **Cho-Pei Jiang:** Writing – review & editing, Software, Resources.

Declaration of competing interest

The authors declare that they have no known competing financial interests or personal relationships that could have appeared to influence the work reported in this paper.

Data availability

Data will be made available on request.

Acknowledgements

Financial support of these studies from Gdańsk University of Technology by the 1/1/2023/IDUB/II.1a/Au+ grant under the Aurum Plus - 'Excellence Initiative - Research University' program is gratefully acknowledged.

References

[1] O. Abdulhameed, A. Al-Ahmari, W. Ameen, S.H. Mian, Additive manufacturing: challenges, trends, and applications, Adv. Mech. Eng. 11 (2019) 1–27, https://doi.org/10.1177/1687814018822880.
[2] Y. Thompson, J. Gonzalez-Gutierrez, C. Kukla, P. Felfer, Fused filament fabrication, debinding and sintering as a low cost additive manufacturing method of 316L stainless steel, Addit. Manuf. 30 (2019) 100861, https://doi.org/10.1016/J.ADDMA.2019.100861.
[3] X. Qi, X. Liang, J. Wang, H. Zhang, X. Wang, Z. Liu, Microstructure tailoring in laser powder bed fusion (L-PBF): strategies, challenges, and future outlooks, J. Alloys Compd. 970 (2024) 172564, https://doi.org/10.1016/J.JALLCOM.2023.172564.
[4] Z. Zhao, L. Wang, D. Kong, P. Liu, X. He, X. Ni, L. Zhang, C. Dong, Texture dependence on the mechanical properties of 18Ni300 maraging steel fabricated by laser powder bed fusion, Mater. Charact. 189 (2022) 111938, https://doi.org/10.1016/J.MATCHAR.2022.111938.
[5] J. Džugan, R. Procházka, M. Koukolíková, S. Rzepa, M. Seifi, J.J. Lewandowski, Assessment of location- and orientation- dependent fatigue behaviour for as-deposited LPBF Inconel 718 using miniaturized specimens, Theor. Appl. Fract. Mech. 133 (2024) 104593, https://doi.org/10.1016/J.TAFMEC.2024.104593.
[6] C.P. Jiang, M. Masrurotin, M. Ramezani, A.T. Wibisono, E. Toyserkani, W. Macek, Sintering parameter investigation for bimetallic stainless steel 316L/inconel 718 composite printed by dual-nozzle fused deposition modeling, Rapid Prototyp J ahead-of-print (2024), https://doi.org/10.1108/RPJ-04-2024-0163.
[7] D. Crisafulli, S. Fintová, D. Santonocito, D. D'Andrea, Microstructural characterization and mechanical behaviour of laser powder Bed Fusion stainless steel 316L, Theor. Appl. Fract. Mech. 131 (2024) 104343, https://doi.org/10.1016/J.TAFMEC.2024.104343.
[8] J. Vishwakarma, R.S. Rajpurohit, G. Sudhakar Rao, K. Chattopadhyay, N.C. Santhi Srinivas, Low cycle fatigue behaviour of additive manufactured maraging steel: Influence of build orientation and heat treatment, Mater. Lett. 350 (2023) 134943, https://doi.org/10.1016/J.MATLET.2023.134943.
[9] A. Karolczuk, A. Kurek, M. Böhm, S. Derda, M. Prażmowski, K. Kluger, K. Żak, Ł. Pejkowski, J. Seyda, Heterogeneous effect of aging temperature on the fatigue life of additively manufactured thin-walled 18Ni300 maraging steel tubular specimen, Mater. Des. 237 (2024) 112561, https://doi.org/10.1016/J.MATDES.2023.112561.
[10] K. Solberg, E.W. Hovig, K. Sørby, F. Berto, Directional fatigue behaviour of maraging steel grade 300 produced by laser powder bed fusion, Int. J. Fatigue 149 (2021) 106229, https://doi.org/10.1016/J.IJFATIGUE.2021.106229.
[11] J. Chen, J. Li, J. Wang, Z. Shi, H. Lin, X. Zhang, Investigation on the characteristics of fracture process zone under cyclic loading: Insights from macro-mesoscopic analysis, Theor. Appl. Fract. Mech. 122 (2022) 103616, https://doi.org/10.1016/J.TAFMEC.2022.103616.
[12] N. Sanaei, A. Fatemi, Analysis of the effect of surface roughness on fatigue performance of powder bed fusion additive manufactured metals, Theor. Appl. Fract. Mech. 108 (2020) 102638, https://doi.org/10.1016/J.TAFMEC.2020.102638.
[13] Y. Bai, C. Zhao, D. Wang, H. Wang, Evolution mechanism of surface morphology and internal hole defect of 18Ni300 maraging steel fabricated by selective laser melting, J. Mater. Process Technol. 299 (2022) 117328, https://doi.org/10.1016/J.JMATPROTEC.2021.117328.

MOST WIEDZY Downloaded from mostwiedzy.pl

[14] S. Romano, P.D. Nezhadfar, N. Shamsaei, M. Seifi, S. Beretta, High cycle fatigue behavior and life prediction for additively manufactured 17–4 PH stainless steel: effect of sub-surface porosity and surface roughness, Theor. Appl. Fract. Mech. 106 (2020) 102477, https://doi.org/10.1016/J.TAFMEC.2020.102477.
[15] K. Slámečka, J. Pokluda, P. Ponížil, S. Major, P. Šandera, On the topography of fracture surfaces in bending-torsion fatigue, Eng. Fract. Mech. 75 (2008), https://doi.org/10.1016/j.engfracmech.2007.01.018.
[16] P. Maruschak, I. Konovalenko, A. Sorochak, Methods for evaluating fracture patterns of polycrystalline materials based on the parameter analysis of ductile separation dimples: A review, Eng. Fail Anal. 153 (2023) 107587, https://doi.org/10.1016/J.ENGFAILANAL.2023.107587.
[17] P. Podulka, W. Macek, D. Rozumek, K. Żak, R. Branco, Topography measurement methods evaluation for entire bending-fatigued fracture surfaces of specimens obtained by explosive welding, Measurement 224 (2024) 113853, https://doi.org/10.1016/J.MEASUREMENT.2023.113853.
[18] W. Macek, R. Branco, M. Korpyś, T. Łagoda, Fractal dimension for bending–torsion fatigue fracture characterisation, Measurement 184 (2021) 109910, https://doi.org/10.1016/J.MEASUREMENT.2021.109910.
[19] G. Macoretta, L. Romanelli, C. Santus, L. Romoli, A.H.A. Lutey, F. Uriati, G. Nicoletto, S. Raghavendra, M. Benedetti, B.D. Monelli, Modelling of the surface morphology and size effects on fatigue strength of L-PBF Inconel 718 by comparing different testing specimens, Int. J. Fatigue 181 (2024) 108120, https://doi.org/10.1016/J.IJFATIGUE.2023.108120.
[20] H. Lauschmann, K. Tesař, K. Jiroušková, Quantitative fractography of fatigue cracks: a new solution in 3D, Procedia Struct. Integ. 23 (2019) 107–112, https://doi.org/10.1016/J.PROSTR.2020.01.071.
[21] H. Lauschmann, F. Šiška, The reference texture: A proposal of a physical explanation, Int. J. Fatigue 43 (2012) 120–127, https://doi.org/10.1016/J.IJFATIGUE.2012.03.002.
[22] S.K. N, A stress-strain function for the fatigue of metals, J. Mater. 5 (1970) 767–778. https://cir.nii.ac.jp/crid/1573668924939429504.
[23] W. Macek, T. Łagoda, N. Mucha, Energy-based fatigue failure characteristics of materials under random bending loading in elastic-plastic range, Fatigue Fract. Eng. Mater. Struct. (2017), https://doi.org/10.1111/ffe.12677.
[24] R. Branco, R.F. Martins, J.A.F.O. Correia, Z. Marciniak, W. Macek, J. Jesus, On the use of the cumulative strain energy density for fatigue life assessment in advanced high-strength steels, Int. J. Fatigue 164 (2022) 107121, https://doi.org/10.1016/J.IJFATIGUE.2022.107121.
[25] Z. Marciniak, R. Branco, W. Macek, M. Dobrzyński, C. Malça, Cyclic deformation and fracture behaviour of additive manufactured maraging steel under variable-amplitude loading, Theor. Appl. Fract. Mech. 129 (2024) 104207, https://doi.org/10.1016/J.TAFMEC.2023.104207.
[26] W. Macek, R. Branco, J. Jesus, J. Costa, S.-P. Zhu, R. Masoudi Nejad, A. Gryguć, Strain energy density and entire fracture surface parameters relationship for LCF life prediction of additively manufactured 18Ni300 steel, Int. J. Damage Mech. (2024), https://doi.org/10.1177/10567895241245879.
[27] W. Macek, D. Rozumek, S. Faszynka, R. Branco, S.P. Zhu, R. Masoudi, Nejad Fractographic-fractal dimension correlation with crack initiation and fatigue life for notched aluminium alloys under bending load, Eng. Fail Anal. 149 (2023), https://doi.org/10.1016/J.ENGFAILANAL.2023.107285.
[28] P. Podulka, W. Macek, B. Zima, G. Lesiuk, R. Branco, G. Królczyk, Roughness evaluation of turned composite surfaces by analysis of the shape of autocorrelation function, Measurement 222 (2023) 113640, https://doi.org/10.1016/J.MEASUREMENT.2023.113640.
[29] W. Macek, R. Branco, P. Podulka, M. Kopec, S.P. Zhu, J. Domingos Costa, A brief note on entire fracture surface topography parameters for 18Ni300 maraging steel produced by LB-PBF after LCF, Eng. Fail Anal. 153 (2023) 107541, https://doi.org/10.1016/J.ENGFAILANAL.2023.107541.
[30] R. Smith, T.H. Watson, T. Topper, A stress-strain parameter for the fatigue of metals, J. Mater. JMLSA 5 (1970) 767–778.
[31] M.A. Miner, Cumulative damage in fatigue, J. Appl. Mech. 67 (1954) AI59–AI64.
[32] D. Kujawski, A deviatoric version of the SWT parameter, Int. J. Fatigue 67 (2014) 95–102, https://doi.org/10.1016/J.IJFATIGUE.2013.12.002.
[33] W. Macek, A. Tomczyk, R. Branco, M. Dobrzyński, A. Seweryn, Fractographical quantitative analysis of EN-AW 2024 aluminum alloy after creep pre-strain and LCF loading, Eng. Fract. Mech. 282 (2023) 109182, https://doi.org/10.1016/J.ENGFRACMECH.2023.109182.
[34] W. Macek, R. Branco, P. Podulka, R. Masoudi Nejad, J.D. Costa, J.A.M. Ferreira, C. Capela, The correlation of fractal dimension to fracture surface slope for fatigue crack initiation analysis under bending-torsion loading in high-strength steels, Measurement 218 (2023) 113169, https://doi.org/10.1016/J.MEASUREMENT.2023.113169.
[35] W. Macek, G. Robak, K. Żak, R. Branco, Fracture surface topography investigation and fatigue life assessment of notched austenitic steel specimens, Eng. Fail Anal. 135 (2022) 106121, https://doi.org/10.1016/J.ENGFAILANAL.2022.106121.

MOST WIEDZY Downloaded from mostwiedzy.pl